Mechanical properties of oxidation-resistant Ni–Cr foams

Heeman Choe, David C. Dunand*

Department of Materials Science and Engineering, Northwestern University, 2225 North Campus Drive, Evanston, IL 60201, USA

Abstract

Reticulated nickel foams were alloyed with chromium by pack-chromizing, resulting in Ni–Cr foams with 9–32 wt.% Cr and 2.6–3.5% relative density. The oxidation resistance at $1000\,^{\circ}C$ of the Ni–Cr foams and the corresponding bulk Ni–Cr alloys is the same, provided the foam's higher surface area is taken into account. The foam compressive yield stress at ambient temperature is in agreement with model predictions. The foam creep behavior, measured between 725 and $825\,^{\circ}C$ in the stress range of 0.1–0.2 MPa, is compared to two models assuming strut compression or strut bending as creep deformation modes. These models, which originally consider dislocation creep as the sole deformation mechanism, are modified to incorporate diffusional creep, due to the relatively fine grain size of the Ni–Cr struts. Good agreement is then found between data and the strut creep compression model.
© 2004 Elsevier B.V. All rights reserved.

Keywords: Metallic foam; Cellular metal; Oxidation; Creep; Strength; Nickel

1. Introduction

Metallic foams have found various applications at ambient temperature due to their excellent density-compensated mechanical properties [1–3]. However, little research has been devoted to their mechanical behavior at elevated temperatures [4–7], despite numerous potential applications, e.g., as the core of sandwich structures in engines and furnaces or as high-temperature catalyst substrate, filter, or heat exchanger. Nickel-base superalloy foams are attractive candidates for such applications, given the excellent mechanical properties and oxidation resistance of superalloys. Superalloy foams have been produced by electron-beam-directed vapor deposition [8], powder sintering [9,10], hollow-sphere sintering [11], and casting [12], but no report of their creep and oxidation resistance was given. Recently, Hodge and Dunand [13] demonstrated that pure Ni foams could be pack-aluminized into homogenous foams with 28–33 wt.% Al, within the single-phase NiAl composition. The creep properties of these reticulated intermetallic foams, with a relative density below 8%, were measured between 800 and

1100 $^{\circ}C$ and found to follow a simple creep model based on compressive deformation of foam struts [5]. Pack cementation was then used by Choe and Dunand [14] to alloy Ni foams with 8–9 wt.% Al or 14–18 wt.% Cr and 5–9 wt.% Al, with a relative density below 3%. After heat-treatment, these foams exhibited the γ/γ' structure typical of nickel-base superalloys, and their creep resistance could be modeled using the strut compression model [14]. For applications where stresses are modest (e.g., substrates, filters, or heat exchangers), creep resistance becomes less important, while oxidation resistance remains a crucial property. A Ni–Cr foam forming a Cr_2O_3 protective layer may be better suited for such applications, given that a binary Ni–Cr foam is easier to synthesize than a ternary superalloy Ni–Al–Cr foams, and also does not necessitate a precipitation heat-treatment.

We show in the present study that the pack-chromizing process, previously demonstrated for ternary Ni–Cr–Al foams with 14–18 wt.% Cr [14], can be used to produce binary Ni–Cr foams with chromium content as high as 32 wt.%. We measure and model the compressive properties of these Ni–Cr foams at both ambient and elevated temperatures. Also, we investigate the oxidation behavior of these foams, which is of both technological interest (for their use in

* Corresponding author. Tel.: +1 847 491 5370; fax: +1 847 467 6573.
  E-mail address: dunand@northwestern.edu (D.C. Dunand).

oxidizing environment at elevated temperature) and of scientific interest (we are aware of only one single report in the literature concerning the solid-state oxidation behavior of metallic foams [15]).

2. Experimental procedures

2.1. Chromizing process

Ni–Cr foams, with a chromium content of 9.2–32.0% (all compositions are given in wt.% unless specified otherwise) and with relative density $\rho^* = 2.6$–3.5%, were created by pack-chromizing of pure Ni foams. These foams (procured from Porvair, Hendersonville, NC) exhibit a reticulated structure consisting of hollow struts with diameter of ca. 224 μm and wall thickness of ca. 84 μm, a cell size of ca. 1.3 mm (20 pores per inch, or 20 ppi) and a relative density of 2.2%. Modifications with respect to the original chromium deposition technique [16,17] used for coating of bulk samples were implemented to achieve a uniform deposition of chromium onto the whole strut surface of the foams. The pack, consisting of 5 wt.% NH_4Cl activator, 25 wt.% Cr powder, and 70 wt.% Al_2O_3 filler powder, was mechanically mixed in a tumbling device for ~20 min. A pure Ni foam (with weight about 1.1 g) was embedded within 40 g of pack contained in a high-chromium stainless-steel bag which was placed in the central zone of a tube furnace with flowing argon as cover gas. Heating and cooling to the process temperature of 1000 °C was performed at a rate of ca. 10 and 7 K/min, respectively. Following chromizing, the samples were weighed to determine chromium mass gain, and then homogenized at 1200 °C for 48 h under flowing Ar, followed by furnace-cooling. A more detailed description of the pack-chromizing procedure is found elsewhere [14,17].

2.2. Oxidation testing

Static oxidation tests were carried out on both unalloyed Ni foams and Ni foams alloyed with 12.2, 19.4, and 27.2% Cr. Small coupons measuring ~13 mm × 13 mm ×7 mm were sectioned from homogenized foam samples, ultrasonically cleaned in water, and then rinsed in ethanol prior to drying in air. After measuring the size and weight of the foam coupons, they were placed on an alumina platen and heated to 1000 °C in static laboratory air at an average rate of 20 °C/min. This temperature was maintained for up to 60 h, with periodic excursions to ambient temperature to measure the weight gain due to oxidation. The weight gain was normalized either by the foam original weight or by their original surface area, which was determined as follows. A pure Ni foam was chromized at 1000 °C for ~3 h, together with a length of pure Ni wire (0.5 mm diameter), whose surface area can be easily calculated. After measuring weight gains for both the foam and the wire, the surface area of the chromized foam was

estimated under the assumption that it is proportional to its weight gain.

2.3. Mechanical testing

Strut microhardness was measured with a Vickers indenter using a 100 g load. Mechanical testing was conducted under compression loading on a servo-hydraulic testing machine with a cross-head speed of 0.1 mm/s using parallelepiped specimens cut to ca. 10 mm × 10 mm × 28 mm by electrodischarge machining, which was used to avoid cell wall damage. The compression testing was performed to a total deformation of over 50%.

Creep tests were performed on two Ni–21%Cr and Ni–29.6%Cr foams under constant compressive uniaxial load, using ~13 mm × 13 mm × 23 mm samples in a compression creep apparatus (Applied Test System, Butler, PA) with a three-zone furnace maintained to a constant temperature value within ±2 °C. Cross-head displacement was measured with a linear voltage displacement transducer outside the hot zone. The minimum creep rate was assessed using a computer program, which calculated the average displacement over a time period long enough to smooth out any noise encountered during the experiment. Deformation in the minimum-rate, secondary-creep region was measured for at least 8 h, after which the specimen was subjected to a higher stress level or a different temperature. The total strain accumulated by the foam specimens did not exceed 20%.

2.4. Metallography

Specimens were mounted in epoxy and polished down to 0.05 μm using standard metallographic procedures. The microstructure was investigated using optical microscopy and SEM, following etching for 20–40 s with a mixture of 10 ml HF and 100 ml HNO_3 for the Ni–Cr foams and for 10–60 s with a mixture of 3 ml HF and 80 ml HNO_3 for the pure Ni foam [18]. The grain size of Ni–Cr foams was determined by drawing 10 random lines of unit length on each examined micrograph and by conducting intercept measurements according to ASTM standards [19].

3. Results

3.1. Processing

Fig. 1(a) shows a cross-section of a hollow triangular strut of the as-received Ni foam, which exhibits a grain size of 13 ± 6 μm. Fig. 1(b) and (c) show optical micrographs for struts of a Ni foam chromized for 2.6 h at 1000 °C (Fig. 1(b)) followed by homogenization for 48 h at 1200 °C (Fig. 1(c)). In Fig. 1(b), the outside surface of the strut is coated with a smooth and continuous Cr-rich deposition layer with an average thickness of ca. 7 μm: a significant amount of the chromium deposited in Fig. 1(b) has thus diffused in the
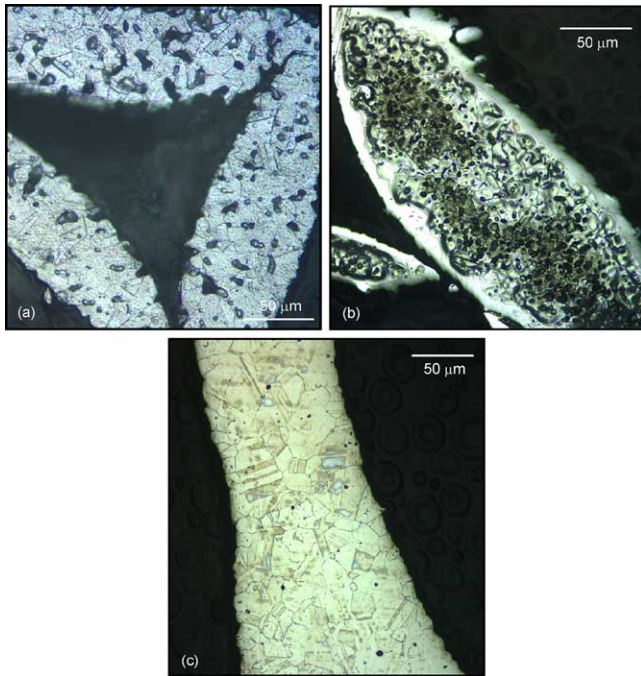
Fig. 1. Optical micrographs for etched cross-section of foam struts of (a) an unalloyed Ni foam (with etch pits) and (b) a foam with average composition Ni–19.2%Cr, after chromizing at 1000 °C for 2.6 h, showing a narrow Cr(Ni) surface layer (arrow) and a Ni(Cr) inner volume (with etch pits); (c) same sample as (b) after homogenization for 48 h at 1200 °C, showing complete dissolution of the Cr(Ni) layer and etched grain boundaries.

nickel, leaving only a thin α-Cr(Ni) outer shell, visible as an un-etched shell in Fig. 1(b), since high-Cr coatings are not attacked by the etchant used here [16]. After homogenization (Fig. 1(c)), the thin α-Cr(Ni) outer layer disappeared, implying that concentration gradients along the strut thickness were removed. The typical diffusion distance calculated using diffusion coefficient of Cr in Ni [20] is $(4Dt)^{1/2} = 177$ μm, much larger than the strut wall thickness of 84 μm, thus implying that the Cr concentration is uniform in the foams after homogenization. The grain size for the homogenized Ni–19.2Cr foam shown in Fig. 1(c) is 24 ± 14 μm.

Fig. 2 is a plot of the time-dependence of Ni foam weight gain upon chromizing at 1000 °C, expressed as average concentration. Chromizing times range from 20 min for 9.2% Cr to 600 min for 32% Cr, well within industrially acceptable times. As expected for a diffusion-controlled mechanism, the chromizing kinetics is monotonously decreasing, as previously found for aluminization and chromizing of similar foams [14]. A more detailed description of the kinetics study can be found elsewhere [13,21].

3.2. Oxidation behavior

Fig. 3 shows the kinetics of mass gain at 1000 °C up to about 50 h for the four Ni and Ni–Cr foams studied. It is apparent that the oxidation kinetics of the Ni foams is significantly slowed by the Cr alloying addition. As compared to the pure
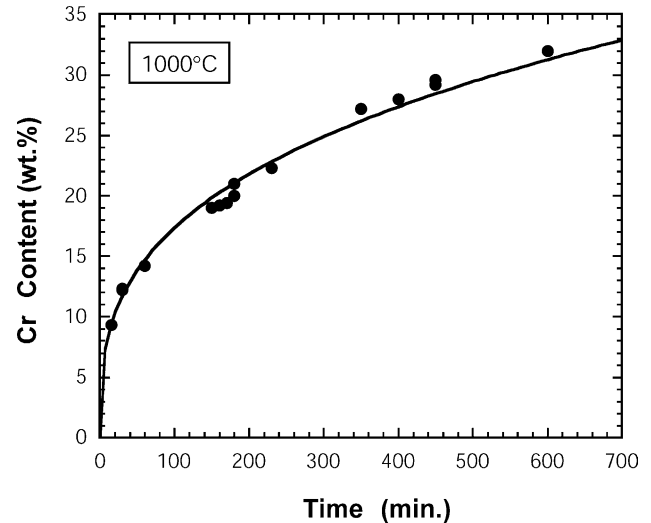

Fig. 2. Time dependence of average composition for Ni foams upon chromizing at 1000 °C.

Ni foam, the weight gain rate of the Ni–19.4%Cr foam is reduced by a factor of two and that of the Ni–27.2%Cr by a factor of four, which is consistent with the trend found in solid Ni–Cr alloys in reference [22]. This is because a rather porous NiO oxide layer develops on the surface of pure nickel, while the Cr_2O_3 oxide layer forming on Ni–Cr alloys is inherently dense and coherent [23,24]. Also, following a rapid increase in mass gain at short times, the oxide layers for all foam compositions grow according to parabolic kinetics: Fig. 3 shows the fitted parabolic curves with the parabolic rate constants (k_p) for times between 5 and 50 h.

Fig. 4 shows the static oxidation curve for the Ni–19.4%Cr foam compared with that for a bulk Ni–20%Cr sample oxidized in pure oxygen [25], normalized either by their weight (Fig. 4(a)) or surface area (Fig. 4(b)). As expected from its
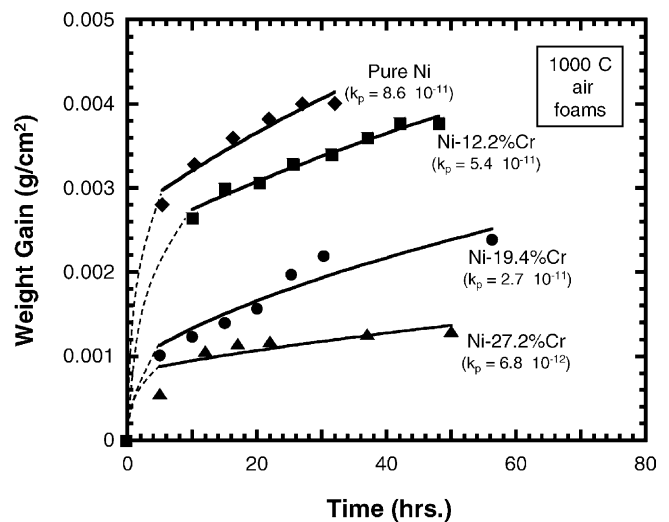

Fig. 3. Kinetics of static air oxidation at 1000 °C for unalloyed Ni foam and Ni–Cr foams with 12.2, 19.4, and 27.2%Cr. Solid lines are parabolic fits with the rate constants (gm^2/cm^4 s) listed in the figure.
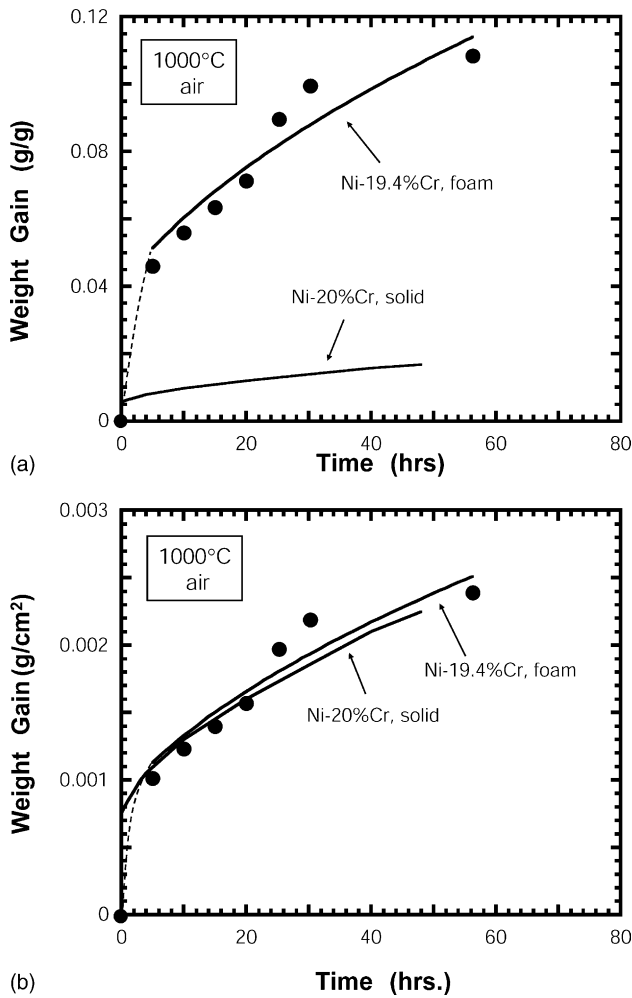
Fig. 4. Kinetics of static oxidation at 1000 °C for a Ni–19.4%Cr foam in air and for bulk Ni–20%Cr in pure oxygen [25], with weight gain normalized by (a) sample weight and (b) sample surface area.

Table 1
Microhardness for struts of heat-treated foams

	Microhardness (HV)
Pure Ni	74.4 ± 3^{a}
Ni–12.3Cr	116 ± 9
Ni–19.4Cr	120 ± 13
Ni–27.2Cr	166 ± 14

[a] As-received foam.

at 900 °C for 66 h [22]. It can thus be safely assumed that the dense oxide layer in Fig. 5 is predominantly Cr_2O_3. Its thickness is about 10% that of the average wall thickness.

3.3. Mechanical properties at ambient temperature

The results of the microhardness tests conducted at room temperature are summarized in Table 1. All indentations were made at least 20 μm away from the nearest cell strut edge. As expected from the solid-solution strengthening effect of chromium in nickel, the strut hardness increases with increasing chromium content.

Compressive stress–strain curves at ambient temperatures for Ni foams with 0–27.2%Cr are shown in Fig. 6(a), where the foam stress is the applied load divided by the specimen cross-sectional area. The pure Ni foam was annealed at 1000 °C for ∼30 min before testing to produce a microstructure comparable to that of the alloyed Ni–Cr foams. All foams display the behavior typical of a ductile metallic foam [27]: linear elasticity at low stresses, followed by a long plastic collapse region where the stress rises slowly, and finally a densification regime where the cell walls start to contact and the stress rises steeply. It is apparent from Fig. 6(a) that increasing the chromium content of the foams leads to an increase in the plastic collapse stress, or foam yield stress, corresponding to the end of the elastic region and start of the plastic collapse region, and determined graphically from the experimental curves as shown in Fig. 6(a).

3.4. Creep properties

The Ni–21%Cr and Ni–29.6%Cr foams displayed a primary creep phase with decreasing strain rate, followed by a secondary creep regime with a minimum strain rate constant over an extended period of time. Fig. 7(a) shows the minimum strain rate $\dot{\varepsilon}$ plotted against the applied stress σ for these foams tested at 825 °C. The creep data follow a power-law.

$$\dot{\varepsilon} = K\sigma^n \exp\left(\frac{-Q}{RT}\right) \tag{1}$$

where K is the Dorn constant, n the stress exponent, Q the creep activation energy, R the gas constant, and T the temperature. The best-fit stress exponents are 3.7 for the Ni–21.0%Cr foam and 3.3 for the Ni–29.6%Cr foam, which are lower than the value reported for Ni–20%Cr bulk alloy ($n = 4.6$) in the temperature range of 680–1160 °C [28]. The narrow range of stresses (0.1–0.2 MPa) measured is due to the following
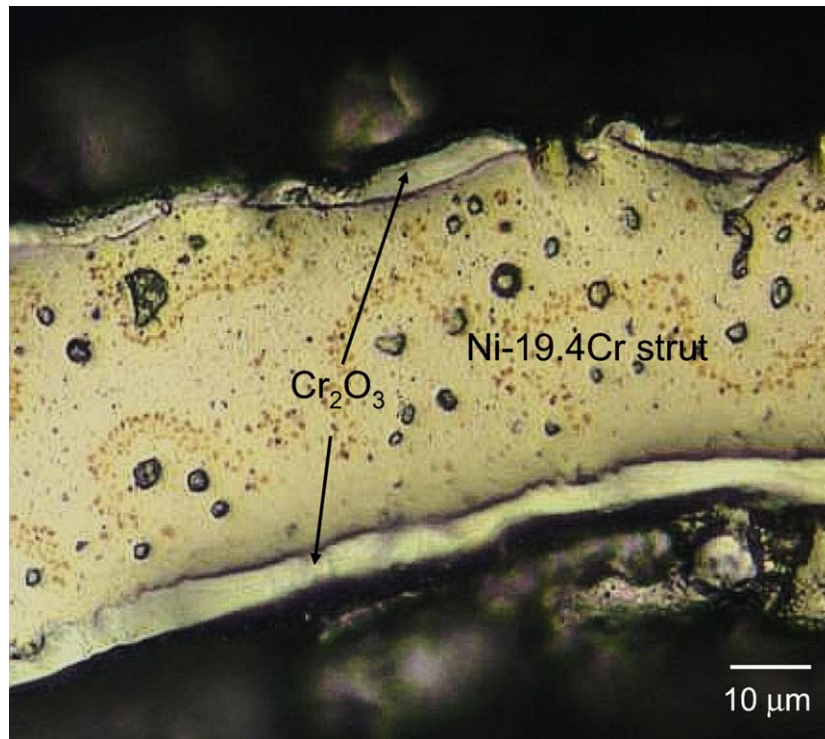
much higher surface area, the Ni–19.4%Cr foam exhibits much faster oxidation kinetics than Ni–20%Cr solid when normalized by weight (Fig. 4(a)). However, no difference is observed, within experimental error, in the oxidation kinetics normalized by surface areas, as shown in Fig. 4(b), indicating that the oxidation mechanism for the foam in air is the same as that for the bulk alloy in pure oxygen.

The high-temperature oxidative resistance of metals depends on the formation of a surface layer (scale) that acts as a barrier to oxygen transport. Shown in Fig. 5 is a nonporous, protective scale of oxide layer, which formed on the surface of a Ni–19.4%Cr foam exposed in air for 55 h. The possible oxide species that can develop on Ni–Cr alloys include NiO, $NiCr_2O_4$, and Cr_2O_3, the prevalence of each varying with oxidation temperature and treatment [24]. However, as temperature increases above ∼800 °C, the formation of chromium oxide (Cr_2O_3) becomes dominant [22,26]. The morphology and dimension of the scale formed on the surface of a Ni–19.4%Cr foam (5–10 μm) at 1000 °C for 55 h is similar to that reported for a Ni–20%Cr bulk alloy (∼8 μm)

Fig. 5. Optical micrograph of cross-section of a strut for a Ni–19.4%Cr foam oxidized in air for ~55 h. A 5 μm thick oxide scale is visible at the strut surfaces (and is missing in some areas due to metallographic preparation).

constraints: stresses higher than 0.2 MPa lead to power-law break-down (as also reported in reference [5] for NiAl foams and [7] for Al foams), while stresses below 0.1 MPa cannot be achieved with the present creep apparatus, due to the weight of the pushrod.

Also shown in Fig. 7(a) are creep data for Ni–8.3%Al and Ni–16.6%Cr–5.5%Al superalloy foams [14], exhibiting creep rates which are lower by one to two orders of magnitude as compared to the Ni–Cr foams, despite their lower relative densities ($\rho^* = 2.5$–2.9% for the superalloy foams versus $\rho^* = 3.0$–3.3% for the Ni–Cr foams). This illustrates the intrinsically better creep resistance of precipitation-strengthened nickel superalloys containing aluminum, as compared to solid-solution-strengthened nickel alloys containing chromium.

Fig. 7(b) shows the minimum strain rate plotted against the inverse of temperature for the Ni–29.6%Cr foam tested at a constant stress, $\sigma = 0.128$ MPa between 725 and 825 °C. Fitting the data to Eq. (1) results in a creep activation energy of 249 kJ/mol. This value is similar to that of bulk Ni–20%Cr (285 kJ/mol) in the temperature range of 680–1160 °C [28].

4. Discussion

4.1. Processing

Besides our previous article on Ni–Cr–Al foams [14], we are aware of only one article where Ni–Cr foams were cre-

ated by pack chromizing of Ni foams [29]: the process temperature was reported as 1100 °C but no information was provided for the process time or the pack composition. The resulting foams exhibited a Cr content of 13–20%, with a higher relative density (5%) and larger cell size (5 mm, corresponding to 5 ppi) than the foams presented here. Other techniques have been proposed for making Ni–Cr foams: sintering of Ni–Cr cut wires [30], electrochemical deposition of Cr upon Ni foams [31], suspension–electrochemical deposition on polymer foams [32], and sintering of Ni–Cr powders [33]. As compared to the cementation technique, the sintered wire or powder foams suffer from low strength (due to the relatively weak sintering necks), and the electrochemically processed foams are prone to contamination from additives used in the bath and possible uneven deposition along the foam struts. The present cementation approach currently consists of two steps (cementation at 1000 °C and homogenization at 1200 °C) which could however easily be combined into a single processing step at an intermediate temperature.

4.2. Oxidation behavior

The parabolic oxidation kinetics of the foams (listed in Fig. 3) at 1000 °C are indicative of a diffusion-controlled process, typical of metals oxidized at elevated temperatures without severe degree of distortion and delamination of the oxide layer [34]. The parabolic rate constants of the foams are in general agreement with those reported in the literature [22].
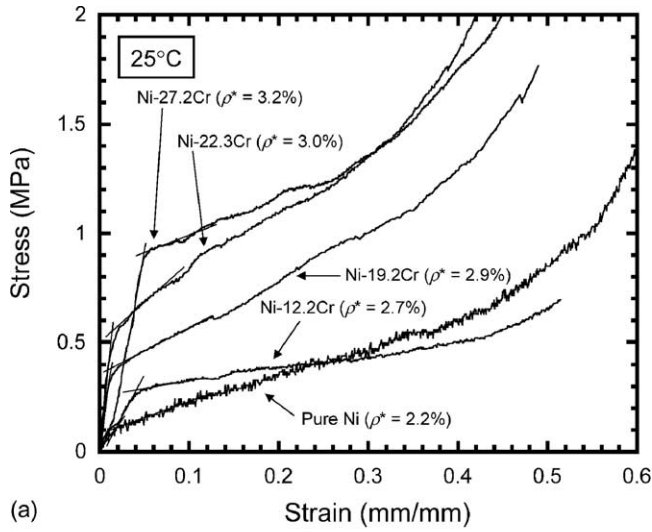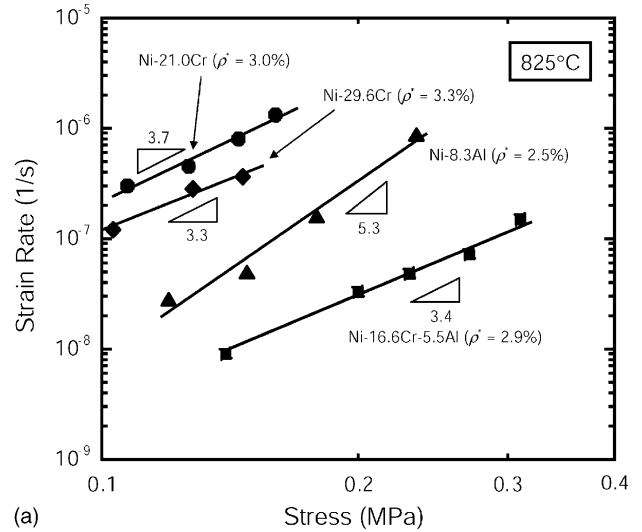
(a)
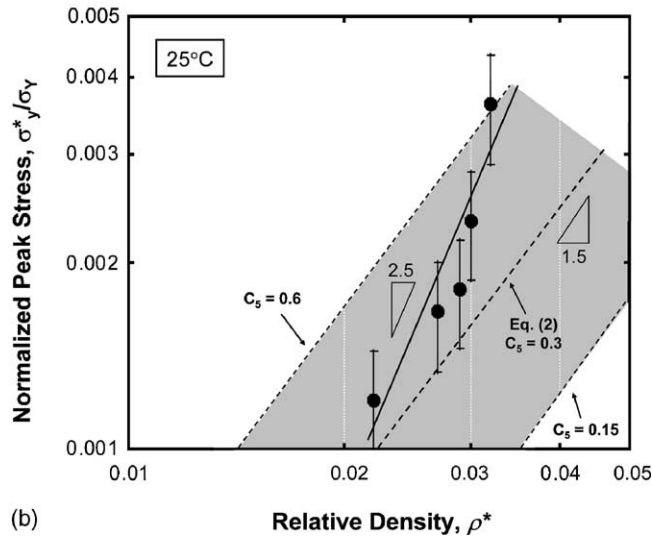
(b)

Fig. 6. (a) Room-temperature compressive stress–strain curves for unalloyed Ni foam (previously annealed 30 min at 1000 °C) and four Ni–Cr foams with 12.2–27.2%Cr foams; (b) plot of foam plastic yield stress (normalized by alloy yield stress) vs. foam relative density, together with predictions from Eq. (2) with $C_5 = 0.15$, 0.3, and 0.6.

(a)

(b)

Fig. 7. (a) Secondary strain-rate plotted against stress at 825 °C for two Ni–Cr foams with 21.0 and 29.6%Cr, showing stress exponents $n = 3.3$–3.7; data for Ni foams with 8.3%Al and 16.6%Cr and 5.5%Al with superalloy microstructures [14] are also shown. (b) Secondary strain-rate plotted against the inverse of temperature at a constant stress of 0.128 MPa for a Ni–29.6%Cr foam, showing an activation energy $Q = 249$ kJ/mol.
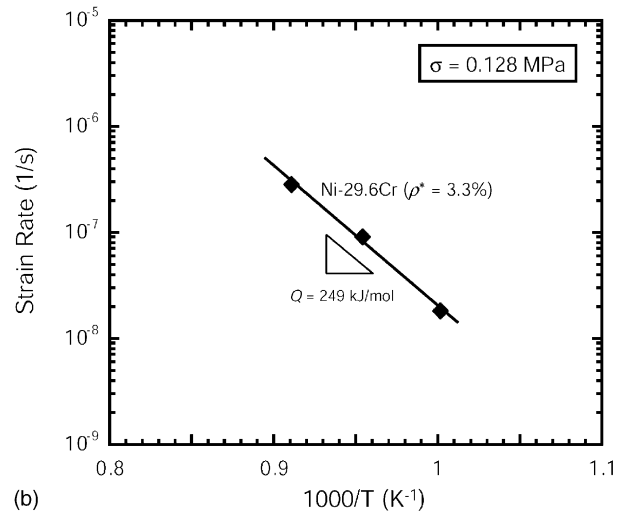
Fig. 3 shows that the oxidation resistance of the Ni foams improves only marginally with the addition of 12.2% Cr, but dramatically with 19.4% Cr. This is in good agreement with the oxidation behavior of solid Ni–Cr alloys which show a significant improvement in oxidation resistance when the chromium content exceeds 15–20% [23], a result attributed to the formation of a very adherent, dense Cr_2O_3 layer. However, the adverse effect of chromium on the oxidation resistance of bulk nickel for chromium content less than ~10 wt.% [22] was not observed for the Ni–12.2% Cr foams examined in the present study.

4.3. Mechanical properties at ambient temperature

As displayed in Table 1, the hardness of the Ni–Cr alloy struts increases as their chromium content increases, as

expected from solid-solution strengthening by chromium in nickel. The hardness increases near linearly with chromium content, similarly to the near linear increase in yield strength reported for bulk Ni–Cr alloys over the same composition range [35] as listed in Table 2.

Fig. 6(a) shows that the yield stress of the foams σ_y^* increases with increasing chromium content, which can be caused both by the increase in foam relative density (following mass gain during the chromizing process) and the increase in metal yield stress by solid-solution strengthening. The relative importance of these two mechanisms is taken into account in a model for the yield stress of open-cell metallic foams developed assuming formation of plastic hinges at the strut joints [1].

$$\sigma_y^* \approx C_5 \sigma_y \rho^{*3/2} \tag{2}$$

Table 2
Yield stress of heat-treated foams at ambient temperature

	Pure Ni	Ni–12.2Cr	Ni–19.2Cr	Ni–22.3Cr	Ni–27.2Cr
Relative density ρ^* (%)	2.2	2.7	2.9	3.0	3.2
Measured foam yield stress σ_y^* (MPa)	0.11[a]	0.29	0.39	0.55	0.91
Alloy yield stress σ_y (MPa) [35]	90	180	220	235	255
Yield ratio σ_y^*/σ_y	0.0012	0.0016	0.0018	0.0023	0.0036

[a] Annealed foam.

where C_5 is a constant in the range of 0.3 and σ_y is the yield strength of the bulk material. Using values of σ_y taken from reference [35] (and listed in Table 2), the normalized foam yield stress σ_y^*/σ_y is plotted against the relative density ρ^* in Fig. 6(b) in a double logarithmic manner, together with the prediction of Eq. (2). The slope of the best-fit curve in Fig. 6(b) is 2.5, which is significantly higher than the value of 1.5 predicted by Eq. (2). However, data are in general agreement with Eq. (2), considering the large experimental error for σ_y^*/σ_y (conservatively estimated as $\pm 20\%$) and the fact that Eq. (2) was found to predict within a factor of ca. 2 the yield stress of aluminum foams with relative densities in the range of 3–40% [36]. This is illustrated in Fig. 6(b), where the experimental data fall within the bounds given by Eq. (2) plotted with $C_5 = 0.15$ and 0.6.

4.4. Creep properties

As for yield strength at ambient temperature, the creep resistance of the Ni–Cr foams is expected to improve with increasing chromium concentrations according to two distinct mechanisms: increased foam relative density and increased solid-solution strengthening. Both effects are captured in a model by Gibson and Ashby [1], who assumed a foam unit cell with joints consisting of two horizontal and one vertical strut. The vertically applied load is transmitted through vertical struts (assumed to remain rigid) to horizontal struts, which deform by creep bending. The foam steady-state creep rate $\dot{\varepsilon}^*$ is then predicted to be

$$\dot{\varepsilon}^* = K \frac{0.6}{(n+2)} \left(\frac{1.7(2n+1)}{n} \right)^n \sigma^{*n} \rho^{*-(3n+1)/2} \exp\left(\frac{-Q}{RT} \right) \tag{3}$$

with the same Dorn constant K, stress exponent n, and activation energy Q as the bulk metal, assumed to deform according to the power-law of Eq. (1). Eq. (3) was developed for solid struts, but the hollow strut geometry of the Ni–Cr foams does not affect the predictions of the creep-bending model appreciably for the present high ratio of wall thickness to strut diameter [37].

Another foam creep model developed by Hodge and Dunand [5] assumes that vertical struts span the whole height of the foam and deform by uniaxial creep compression, while horizontal struts remain rigid, and only prevent buckling of the vertical struts. The foam creep rate $\dot{\varepsilon}^*$ is given as

$$\dot{\varepsilon}^* = K \left(\frac{\rho^*}{3} \right)^{-n} \sigma^{*n} \exp\left(\frac{-Q}{RT} \right) \tag{4}$$

Creep parameters measured for a Ni–20%Cr bulk alloy [28] ($n = 4.6$, $Q = 285$ kJ/mol, and $K = 3.8$ MPa$^{-4.6}$ s^{-1}) are used to plot the creep rates predicted from Eqs. (3) and (4) for the Ni–21.0%Cr and Ni–29.6%Cr foams in Fig. 8(a) and (b), respectively. The creep rates predicted by the bending model (Eq. (3)) are over three orders of magnitude higher than for the compression model (Eq. (4)), as also reported in our previous studies of NiAl, Ni–Al, and Ni–Cr–Al foams [5,14].
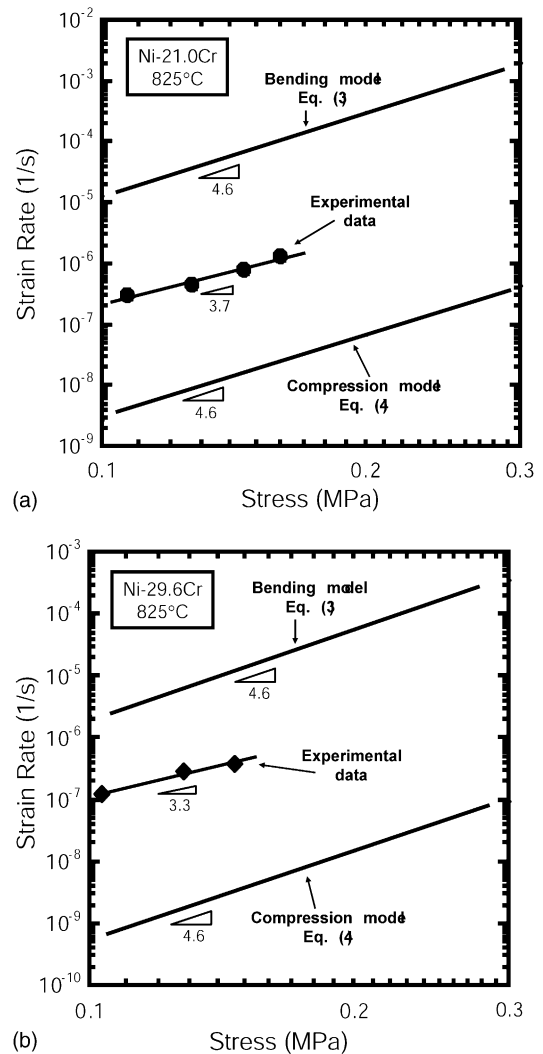

Fig. 8. Comparison of the experimental creep data for (a) Ni–21.0%Cr and (b) Ni–29.6%Cr foams at 825 °C and predictions from analytical calculations based on the bending of struts [Eq. (3)] and creep compression of struts [Eq. (4)], assuming dislocation creep.

This is because the two models represent extreme cases: the bending model corresponds to a weak foam geometry where three struts converge into each cell joint, whereas the creep compression model is for a strong geometry where six struts converge into each joint. In general, real foams with complex cell architecture will exhibit a mixture of both bending and uniaxial compression in their struts, so that experimental values are expected to fall between the two predictions. Previous studies on NiAl, Ni–Al, and Ni–Cr–Al reticulated foams [5,14] have shown experimental values to be much closer to the compression model than to the bending model. In the present case, the logarithm of the creep rates of the Ni–Cr foams falls half way between the predictions of both models (Fig. 8(a) and (b)). Also, the stress exponent of the foam is different from that of the bulk alloy ($n = 3.3$–3.7 versus $n = 4.6$). These discrepancies may be explained by the presence of an additional creep mechanism as discussed below.

The Ni–Cr bulk alloys studied by Monma et al. [28] exhibited an average grain size of 400–450 μm, which is much larger than that of the present Ni–Cr foams (24 $\pm$ 14 μm for the Ni–19.2%Cr foam, Fig. 1(c)). Therefore, diffusional creep processes active for materials with small grains should also be considered. The diffusional creep rate equation is given as [38]

$$\dot{\varepsilon} = \frac{14\sigma\Omega}{\kappa T d^2} D_{\mathrm{eff}} \qquad (5)$$

where Ω is the atomic volume, κ the Boltzman constant, d the grain size, and the effective diffusion coefficient is given by

$$D_{\mathrm{eff}} = D_{\mathrm{v}} \left[1 + \frac{\pi}{d} \frac{\delta D_{\mathrm{b}}}{D_{\mathrm{v}}} \right] \qquad (6)$$

with D_{v} as the diffusion constant for lattice diffusion of nickel, and δD_{b} the diffusion constant for boundary diffusion. All the above parameters are given in reference [38] for Ni–20%Cr and assumed to be unchanged for Ni–30%Cr (based on the small or inexistent variability in these parameters between Ni–10%Cr and Ni–20%Cr [38]). For the relatively low temperatures and small grain sizes of the present study, the volume diffusion is much lower than the boundary diffusion, indicating that Coble creep dominates Nabarro–Herring creep in the struts of the Ni–Cr foams.

Replacing the power-law (Eq. (1)) for dislocation creep with the Newtonian flow law (Eq. (5)) for diffusional creep in the derivation of the foam creep models results in the following equations for the strut bending model:
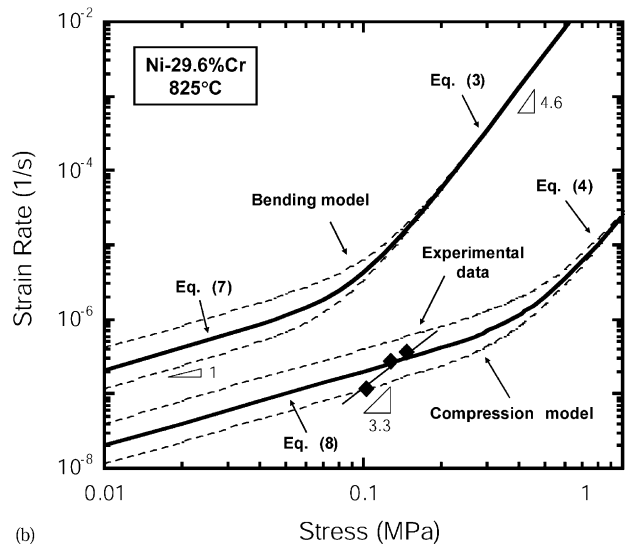
$$\dot{\varepsilon}^* = \frac{14.3\Omega}{\kappa T d^2} \sigma^* \rho^{*-2} D_{\mathrm{eff}} \qquad (7)$$

and for the strut compression model:

$$\dot{\varepsilon}^* = \frac{14\Omega}{\kappa T d^2} \sigma^* \left(\frac{\rho^*}{3} \right)^{-1} D_{\mathrm{eff}} \qquad (8)$$
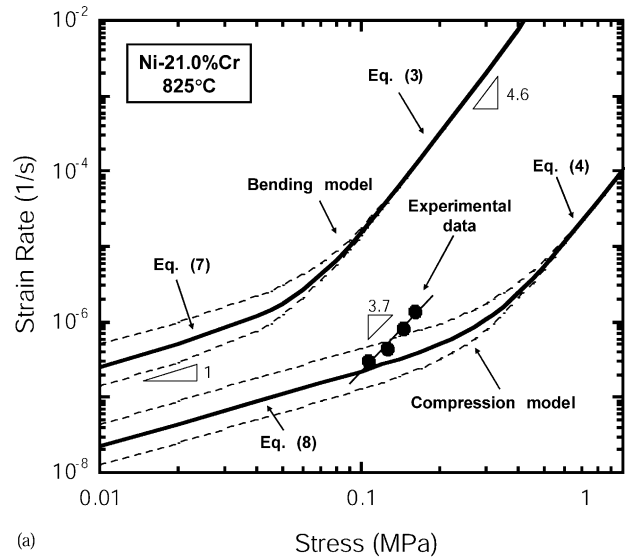
Fig. 9. Comparison between experimental creep data for the (a) Ni–21.0%Cr ($\rho^* = 3\%$) and (b) Ni–29.6%Cr ($\rho^* = 3.3\%$) foams at 825 °C and predictions from analytical models based on creep bending or creep compression, after combining both dislocation creep and diffusional creep processes. Dislocation creep is dominant at high stresses and diffusional creep at lower stresses. Solid lines represent predictions with an average grain size of 24 μm and dotted lines positive (29 μm) or negative (19 μm) deviations.

Because dislocation creep and diffusional creep are independent processes, their rate equations can be added to obtain the overall creep rate of the foams. This is done in Fig. 9(a) and (b) for the creep bending model (sum of Eqs. (3) and (7)) and the creep compression model (sum of Eqs. (4) and (8)). As expected, dislocation creep dominates at high stresses and diffusional creep at low stresses. The experimental data are near the transition region where both mechanisms contribute significantly to the overall foam creep rate, in the vicinity of 0.04–0.15 MPa for the bending model and 0.2–0.8 MPa for the compression model in Fig. 9(a). In this transition region, the stress exponent is expected to vary between $n = 1$

(for diffusional creep) and $n = 4.6$ for dislocation creep. The foams stress exponent is indeed intermediate between these values ($n = 3.7$ for Ni–21.0%Cr and $n = 3.3$ for Ni–29.6%Cr foams). Within the error bands given by the uncertainty in grain size (estimated to be ± 5 micrometers), the creep compression model is in agreement with the experimental creep data, but the creep bending model significantly over-predicts the data. A similar situation was reported for the power-law creep behavior of NiAl, Ni–Al, and Ni–Cr–Al reticulated foams [5,14] created by pack-cementation from the same Ni foams. It was then noted that both models are valid, but represent extreme cases: foams with few struts converging into nodes will exhibit mostly bending in their struts, so that Eqs. (3) and (7) are expected to provide a good approximation of their creep behavior. Foams with many struts converging into nodes will deform primarily by strut compressive deformation, and their creep behavior will be more closely approximated by Eqs. (4) and (8).

We note that the above equations assume simple, idealized cell geometries which cannot capture the complex deformation occurring within the present foams: spatial variations in strut cross-section, orientation, connectivity, composition, and grain size all result in a distribution of strain rates within the foam, for which only the volume-averaged rate is measured experimentally. More complex finite-element models are needed to quantify these variations, but the idealized foam creep equations (Eqs. (3), (4), (7) and (8)) provide simple estimations capturing basic differences in foam geometry and creep mechanisms.

In summary, it appears that the present Ni–Cr foams are deforming by a combination of dislocation creep and diffusional creep at 825 °C for stresses between 0.1 and 0.2 MPa. The foam creep equations based on strut compressive deformation seem to explain quantitatively and without adjustable parameters the behavior of the present foams, within a relatively large experimental error. To confirm the validity of the diffusional creep equations (Eqs. (7) and (8)), further experiments at lower stresses, lower temperatures, and/or lower grain size are needed to access a regime where diffusional creep is the sole dominant deformation mechanism.

5. Conclusions

Reticulated Ni–Cr foams with 9–32 wt.% Cr and relative densities $\rho^* = 2.6$–3.5% were created by a pack-chromizing method. Their mechanical and oxidative properties were studied, leading to the following conclusions:

1. At ambient temperature, the foam compressive yield stress increases with chromium content, as a result of increases in both foam relative density and strut yield strength due to solid solution strengthening. The data are in general agreement with an existing model.
2. The oxidation kinetics of the foam is similar to those of the corresponding bulk Ni–Cr alloys, after taking into account the higher foam surface area.
3. Creep tests performed on Ni–21.0%Cr and Ni–29.6%Cr foams at 825 °C indicate that the foam with higher Cr content is more creep resistant, probably for the same reasons mentioned in point 1 above for the increased yield strength.
4. Introducing power-law creep parameters from Ni–Cr bulk alloys of similar composition into two analytical creep foam equations (based on struts deforming by bending or compression by dislocation creep) provides predictions which bracket the experimental creep data for the two Ni–Cr foams; the creep exponent of the foams ($n = 3.3$–3.7) is however smaller than that of the base alloys ($n = 4.6$).
5. The relatively small grain size of the Ni–Cr foam struts indicates that diffusional creep may be dominant at low stresses. The above two equations are modified to incorporate the contribution of diffusional creep. The experimental data are then, within experimental error, in quantitative agreement with the creep compression model in the range where both diffusional and dislocation creep are significant, while the creep bending model significantly underestimates the creep resistance of the foams. Further experiments at lower stresses will be needed to probe the validity of the foam diffusional creep equations.

Acknowledgements

References

[1] L.J. Gibson, M.F. Ashby, Cellular Solids: Structure and Properties, Pergamon Press, Oxford, 1988.
[2] H.P. Degischer, B. Kriszt, Handbook of Cellular Metals: Production, Processing Applications, Wiley-VCH, Weinheim, 2002.
[3] M.F. Ashby, T. Evans, N.A. Fleck, J.W. Hutchinson, H.N.G. Wadley, Metal Foams: a Design Guide, Butterworth-Heinemann, Boston, 2000.
[4] E.W. Andrews, J.S. Huang, L.J. Gibson, Acta Mater. 47 (1999) 2927.
[5] A.M. Hodge, D.C. Dunand, Metall. Mater. Trans. 34A (2003) 2353.
[6] E.W. Andrews, L.J. Gibson, M.F. Ashby, Acta Mater. 47 (1999) 2853.
[7] P. Zhang, M. Haag, O. Kraft, A. Wanner, E. Arzt, Philos. Mag. 82A (2002) 2895.
[8] D.T. Queheillalt, D.D. Hass, C.J. Sypeck, H.N.G. Wadley, J. Mater. Res. 16 (2001) 1028.
[9] D.T. Queheillalt, Y. Katsumura, H.N.G. Wadley, Scripta Mater. 50 (2004) 313.
[10] M. Bram, C. Stiller, H.P. Buchkremer, D. Stöver, H. Baur, Adv. Eng. Mater. 2 (2000) 196.
[11] D.J. Sypeck, P.A. Parrish, H.N.G. Hayden, in: D.S. Schwartz, D.S. Shih, H.N.G. Wadley, A.G. Evans (Eds.), Porous and Cellular Materials for Structural Applications, MRS, Warrendale, PA, 1998, p. 205.

[12] J. Gayda, S. Padula, Internal Report, NASA/TM (2001-211305), Cleveland, OH, 2001.

[13] A. Hodge, D.C. Dunand, Intermetallics 9 (2001) 581.

[14] H. Choe, D.C. Dunand, Acta Mater. 52 (2004) 1283.

[15] A. Leonov, A. Romashko, in: J. Banhart, N.A. Fleck, A. Mortensen (Eds.), Proceedings of the Third International Conference on Cellular Metals and Metal Foaming Technology, Berlin, Germany, 2003, p. 271.

[16] F.D. Geib, R.A. Rapp, Oxid. Met. 40 (1993) 213.

[17] E. Godlewska, K. Godlewski, Oxid. Met. 22 (1984) 117.

[18] G.F. Vander Voort, Metallography: Principles and Practice, McGraw-Hill, New York, NY, 1999.

[19] Annual Book of ASTM Standards, ASTM, Philadelphia, PA, 2000, p. 3.01.

[20] C.J. Smithells, Metals Reference Book, Butterworth-Heinemann, Oxford, UK, 1992.

[21] D.C. Dunand, A.M. Hodge, C. Schuh, Mater. Sci. Tech. 18 (2002) 326.

[22] C.S. Giggins, F.S. Pettit, Trans. Met. Soc. AIME 245 (1969) 2495.

[23] O. Kubaschewski, B.E. Hopkins, Oxidation of Metals and Alloys, Butterworths, London, UK, 1962.

[24] F. Pedraza, M. Reffass, J. Balmain, G. Bonnet, J.F. Dinhut, Mater. Sci. Eng. 357A (2003) 355.

[25] J.M. Hampikian, D.I. Potter, Oxid. Met. 38 (1992) 139.

[26] G. Calvarin, R. Molins, A.M. Huntz, Oxid. Met. 53 (2000) 25.

[27] J.T. Beals, M.S. Thompson, J. Mater. Sci. 32 (1997) 3595.

[28] K. Monma, H. Suto, H. Oikawa, J. Jpn. Inst. Met. 28 (1964) 253.

[29] V.V. Skorokhod, A.N. Leonov, S.M. Solonin, V.K. Sul'zhenko, V.P. Katashinskii, I.G. Slys', A.E. Rutkovskii, V.A. Barabash, Powder Metall. Met. Ceram. 41 (2002) 253.

[30] L.I. Kartashova, V.I. Salo, Met. Sci. Heat Treat. 34 (1992) 290.

[31] V.V. Kamelin, V.I. Kichigin, V.N. Antsiferov, O.P. Koshcheev, Russ. J. Appl. Chem. 71 (1998) 257.

[32] V.D. Khramtsov, Powder Metall. Met. Ceram. 40 (2001) 208.

[33] S.M. Solonin, V.P. Katashinskii, O.I. Get'man, Powder Metall. Met. Ceram. 42 (2003) 235.

[34] ASM-Handbook: Heat Treatment, Structure and Properties of Non-ferrous Alloys, ASM, Metals Park, OH, 1984.

[35] R.M.M. Pelloux, N.J. Grant, Trans. Met. Soc. AIME 218 (1960) 232.

[36] E.W. Andrews, W. Sanders, L.J. Gibson, Mater. Sci. Eng. 270A (1999) 113.

[37] K.C. Goretta, R. Brezny, C.Q. Dam, D.J. Green, A.R. De Arellano-Lopez, A. Dominguez-Rodriguez, Mater. Sci. Eng. 124A (1990) 151.

[38] H.J. Frost, M.F. Ashby, Deformation-Mechanism Maps: the Plasticity and Creep of Metals and Ceramics, Pergamon Press, New York, NY, 1982.